

A lithographically-patterned, elastic multi-electrode array for surface stimulation of the spinal cord

Kathleen W. Meacham · Richard J. Giuly · Liang Guo · Shawn Hochman · Stephen P. DeWeerth

© Springer Science + Business Media, LLC 2007

Abstract A new, scalable process for microfabrication of a silicone-based, elastic multi-electrode array (MEA) is presented. The device is constructed by spinning poly (dimethylsiloxane) (PDMS) silicone elastomer onto a glass slide, depositing and patterning gold to construct wires and electrodes, spinning on a second PDMS layer, and then micropatterning the second PDMS layer to expose electrode contacts. The micropatterning of PDMS involves a custom reactive ion etch (RIE) process that preserves the underlying gold thin film. Once completed, the device can be removed from the glass slide for conformal interfacing with neural tissue. Prototype MEAs feature electrodes smaller than those known to be reported on silicone substrate (60 μm diameter exposed electrode area) and were capable of selectively stimulating the surface of the *in vitro* isolated spinal cord of the juvenile rat. Stretchable serpentine traces were also incorporated into the functional PDMS-based MEA, and their implementation and testing is described.

Keywords Poly(dimethylsiloxane) · Multi-electrode array · Neural prosthetic · Spinal cord · Neural interfacing · Electrophysiology · Surface stimulation · Neural control · Spinal cord injury

KWM and RJG contributed equally to the work reported in this manuscript.

K. W. Meacham · R. J. Giuly · L. Guo · S. P. DeWeerth (✉)
Wallace H. Coulter Department of Biomedical Engineering,
Georgia Institute of Technology and Emory University,
313 Ferst Drive,
Atlanta, GA 30332, USA
e-mail: steve.deweerth@bme.gatech.edu

S. Hochman
Department of Physiology, Emory University School of Medicine,
615 Michael St.,
Atlanta, GA 30322, USA

1 Introduction

Neural prostheses (NPs) that electrically activate central and peripheral systems have shown significant promise in supplementing function lost to disease or injury (Chapin 2000; Prochazka et al. 2001; Stein and Mushahwar 2005). Clinical advancements made possible by NP technology include those that restore hearing (Clark et al. 1977; Kessler 1999; Spelman 1999), respiration (DiMarco 2001), bladder voiding (Brindley et al. 1982; Grill et al. 2001), and upper and lower extremity control (Kraft et al. 1992; Kralj et al. 1988; Liberson et al. 1961; Prochazka et al. 1997; Taylor et al. 1999; Weingarden et al. 1998). A subset of these prostheses communicates with neural tissue via penetrating multiple-electrode arrays (MEAs), which can provide highly specific and robust activation of the targeted neurons (Branner et al. 2001; Hillman et al. 2003; McDonnall et al. 2004; Tyler and Durand 2002). Multi-electrode NPs that penetrate neural tissue, however, have been shown to incur acute and chronic damage, which in turn can result in degradation of both the interfaced tissue and the implanted device (Edell et al. 1992; Polikov et al. 2005; Schmidt et al. 1993). There has been a variety of successful efforts to minimize the adverse effects of MEA invasiveness, including those using specialized device geometries and protective surface coatings (He and Bellamkonda 2005; Holman et al. 2002; Naples et al. 1988; Zhong et al. 2001).

The damage sustained by NP interfacing can be minimized by stimulating exclusively from the surface of the interfaced neural tissue. This approach eliminates damage associated with electrode penetration, but potentially loses direct accessibility to the targeted neuronal circuitry. For certain prosthetic applications, however, this loss in accessibility can be ameliorated by the inherent organization of the neuronal systems. For example, the sub-

fascicular organization of the peripheral nerve has been successfully tapped into by surface electrodes to elicit functionally-specific muscle activation (Leventhal and Durand 2003, 2004). In an analogous manner, spinal-cord NPs might utilize the topographical organization of spinal axons into bundles (i.e., white matter tracts) to recruit specific motor outputs via surface stimulation. The relevance of this approach has been supported by studies in which spinal cord surface stimulation has been used effectively to elicit coordinated motor responses—including locomotion—in both rats and humans (Gerasimenko et al. 2006; Ichiyama et al. 2005; Magnuson et al. 1995; Magnuson and Trinder 1997).

The specificity with which surface-stimulating NPs activate neural circuitry may also be augmented by tailoring the electrode's physical properties for optimal tissue interfacing. A critical factor in this interaction specificity is the degree of isolation between electrodes and their targeted neural tissue, which should be minimized to reduce signal leakage to adjacent tissue and extracellular space (Loeb and Peck 1996; Stein and Pearson 1971; Struijk et al. 1999). For this reason, surface-stimulating MEAs whose designs confer a closer fit of their electrodes to the tissue surface may have potential for improving the selectivity with which their targeted neural systems are activated. Towards this end, numerous MEAs have been developed with specialized flexible substrates. Table 1 is a summary of some of the more recently reported flexible-substrate, multi-electrode NP technologies, which use as substrates the biocompatible polymers polyimide, parylene, and polydimethylsiloxane (PDMS).

The MEA substrate PDMS, with a Young's modulus of 0.4–1.0 MPa, is significantly more elastic than parylene and polyimide, whose Young's moduli are approximately 4–4.5 and 2.3–2.8 GPa, respectively (Armani et al. 1999; Rousche et al. 2001; Suzuki 2003; Yang et al. 1998). Because of its greater elasticity, PDMS can confer not just flexible but also conformable interfacing with neural tissue. In addition, the oxygen-permeability and improved mechanical impedance matching properties of PDMS have

potential to augment the viability of the MEA/neural tissue interface. Other groups have demonstrated successes fabricating PDMS-based MEAs for activation and recording of neural circuitry (Cater et al. 2007; Leventhal and Durand 2004; Maghribi et al. 2002; Schuettler et al. 2005); however, these MEAs have not been able to achieve the same electrode size resolution as demonstrated in polyimide and parylene MEAs.

In this paper, we present the design, fabrication, and preliminary testing of an elastic MEA with electrode diameters (<60 μm) smaller than previously reported using a PDMS substrate. To achieve this feature size, we implement a novel, customized Reactive Ion Etch (RIE) fabrication process. Our functional PDMS-based array exhibits properties that enable close, mechanically conformable contact with the surface of the spinal cord for selective stimulation of axonal tracts. To confer an even greater elasticity, we implement a serpentine pattern that allows the traces to stretch along with the PDMS substrate; this helps us to minimize electrode trace elasticity issues seen with previous fabrication techniques (Maghribi et al. 2002; Schuettler et al. 2005).

2 Fabrication process

Our fabrication approach consists of layering patterned gold between two thin sheets of PDMS and using a novel reactive ion etch (RIE) step to expose the gold electrode contacts. We eliminate the need for gold-to-PDMS adhesion by bordering exposed electrode contacts with PDMS, which prevents the gold from lifting off. As a means to pattern the gold electrodes, we use standard photolithography because it can generate small features reliably. To create orifices in the upper PDMS layer, we use a protective aluminum mask layer along with RIE techniques. Our fabrication steps use standard microfabrication techniques on a novel (PDMS) substrate and are designed to enable scaling of the MEA to a very large number of small-feature size (<60 μm diameter) electrodes.

Table 1 Comparison of MEA technologies for surface stimulation of neural tissue

Source/type of MEA	Reported electrode size (μm)	Substrate material	Interfaced neural tissue type
(Stieglitz 2001)	10 μm diameter	Polyimide	Various
(Rodger et al. 2006)	150 μm diameter	Parylene	Spinal cord and Retina
(Maghribi et al. 2002)	300–350 μm diameter	PDMS	Retina
(Schuettler and Stieglitz 2000)	500 μm diameter	Polyimide-PDMS hybrid	Radial nerve
(Sahin et al. 1997)	500 μm by 1 mm rectangular	PDMS	Peripheral nerves
(Tsay et al. 2005)	100 μm –1 mm squares	PDMS	Hippocampal culture
(Schuettler et al. 2005)	600 μm square	PDMS	Various

2.1 Fabrication step 1. Preparation of PDMS and rigid substrate

To prepare the elastomer substrate, we mix PDMS (Sylgard 184©, Dow Corning) at 10:1 PDMS prepolymer to curing agent ratio and store the mixture at $-20\text{ }^{\circ}\text{C}$ to slow curing. The cooled mixture remains liquid for several days. No degassing under vacuum is required because air bubbles rise out during the first 5 h of storage. Prior to use, we allow the mixture to sit at room temperature for 15 min to reduce the formation of condensation.

We use a $75\times 50\times 1\text{ mm}$ glass slide as a rigid substrate for fabrication, and prepare it through sequential rinsing with trichloroethylene, acetone, isopropanol, and deionized water. We then evaporate 250 \AA of gold onto the slide to create a non-stick layer (Fig. 1(a)). All evaporation is performed with a CVC Products, Inc. Electron Beam Evaporator. The initial gold layer facilitates future removal of the finished elastomer-based array from the glass slide, a technique originally described by Maghribi et al. (2002) for their retinal array. Prior to the evaporation step, we place transparent adhesive tape around the perimeter of the glass slide to form a 3 mm-thick border. After removing the tape, the bare glass bonds to the subsequent PDMS layer more strongly than to the anti-adhesion gold layer. This configuration prevents fabrication chemicals from seeping under the array, which subsequently prevents the device from delaminating off the glass slide during processing.

2.2 Step 2. Creation of PDMS base layer

Following removal of the adhesive tape border, we spin the PDMS mixture onto the slide at 1,500 rpm for 15 s, using a 1,000 rpm/s ramp rate. We then allow the PDMS layer to

settle for 1 min and cure it in a $95\text{ }^{\circ}\text{C}$ oven for 15 min. This produces a PDMS film approximately $70\text{ }\mu\text{m}$ thick (Fig. 1(b)).

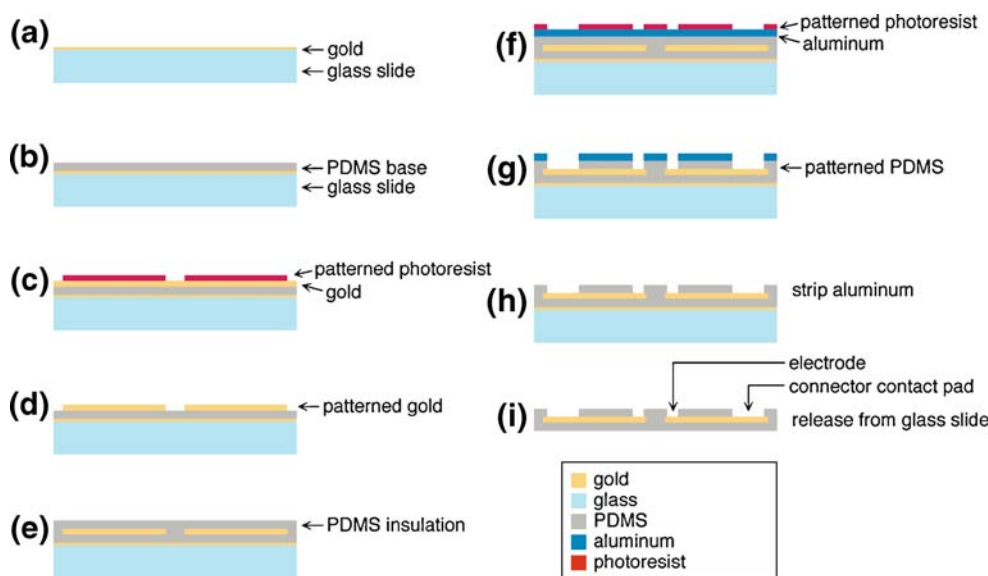
2.3 Step 3. Deposition and patterning of gold film

To create the electrodes and wire traces, we first evaporate a $5,000\text{ \AA}$ thick gold film onto the PDMS layer. $5,000\text{ \AA}$ was found to be the maximum thickness achievable by a single evaporation step while maintaining good film quality. We use this maximal thickness in order to improve the robustness of the MEA, which ultimately must survive the mechanical stresses and electrolytic corrosion of repetitive, long-term use. Following evaporation of the gold film, we use standard photolithography techniques to transfer the electrode pattern into a positive photoresist (Shipley Microposit 1813) (Fig. 1(c)). We etch the gold layer by first dipping the patterned device in Transene GE-8148 Gold Etchant and then rinsing it in DI water. Because no adhesion layer is used between the gold and PDMS, we avoid delamination by spin drying the device at 2,000 rpm for 30 s rather than jet drying with a nitrogen gun. In addition, we flood expose the sample (no mask used) and then soak it in developer (Microposit MF319) to remove the photoresist (Fig. 1(d)). These steps eliminate the need for solvent strippers (e.g. acetone) that can swell the PDMS. After removing the photoresist, we rinse the sample again by dipping in water and then we spin dry and bake at $80\text{ }^{\circ}\text{C}$ to remove moisture.

2.4 Step 4. Creation of PDMS insulating layer

To create the second layer of PDMS, we spin the PDMS mixture onto the patterned gold at 6,000 rpm for 150 s, with a 1,000 rpm/s ramp rate. This film is then cured in an oven

Fig. 1 Fabrication Steps for a PDMS-Substrate Multi-Electrode Array (MEA): (a) Deposition of gold anti-adhesion layer onto glass slide. (b) Spin coating of PDMS. (c) Gold conductor layer deposition and positive photoresist defining conductor pattern. (d) Etching of gold and photoresist removal. (e) Spin coating of insulating PDMS. (f) Aluminum deposition for RIE mask and photoresist defining the mask pattern. (g) Etching of Aluminum and reactive ion etching to remove PDMS. (h) Stripping of aluminum. (i) Removal from glass slide



for 24 h at 95 °C to create a thin PDMS layer of approximately 9.5 μm (Fig. 1(e)).

2.5 Step 5. Deposition and patterning of aluminum mask layer

To protect the PDMS surface during the ensuing reactive ion etch (RIE) step, we deposit and pattern an aluminum mask. We accomplish this by evaporating aluminum (1,500 Å at 0.5 Å/s) onto the PDMS and then patterning with positive photoresist. For accurate placement of the holes above the gold electrodes, we carefully align our second mask to gold-patterned alignment marks under the PDMS. These alignment marks have been protected during the aluminum evaporation using transparent adhesive tape, which is subsequently removed. The protective mask pattern is then defined using Transene Type A aluminum etchant.

2.6 Step 6. Reactive ion etch (RIE)

To create openings in the upper PDMS layer for the gold electrodes and electrical contacts, we use a custom two-step reactive ion etch (RIE) process (Plasma-Therm Reactive Ion Etcher). During this dry etching, the aluminum layer serves as a protective mask and the gold film acts as an etch-stop layer. The first of our two steps uses a 10% CF_4 and 90% O_2 mixture for 240 min (Table 2b); this step etches through most of the PDMS and strips away the photoresist. For our second step, a 3% CF_4 and 97% O_2 mixture (Table 2c) is applied for 150 min to etch any remaining PDMS without damaging the underlying gold (Fig. 1(g) and Fig. 2).

We use RIE parameters modified from a rate-optimized PDMS etch recipe developed by previous research (Table 2a) (Garra et al. 2002; Shao and Miller 2007). These previously-established parameters were optimized more for speed than selectivity and were not suitable for our purpose because they attack the underlying gold film. To cleanly etch away the PDMS film while leaving the gold layer intact, we use the following modifications: (1) We decrease CF_4 concentration and increase oxygen to elimi-

nate the tendency to redeposit polymer (Madou 2002), (2) We reduce the power and increase the pressure, under the assumption that a more chemical—rather than physical—etching process would have less effect on gold and therefore tend to etch PDMS with more selectivity, and (3) We use two etching steps: one that removes the bulk of the PDMS (Table 2b) and another slower etch that cleans off any residue without attacking gold at an appreciable rate (Table 2c).

We use a dry etch process to open the orifices in the PDMS insulating film because wet etching of PDMS can be more difficult to control (Maghribi et al. 2002). We suspect that Recipe A etches the patterned gold layer while the film of PDMS remains on top of it, and that this phenomenon is related to the gas-permeable properties of PDMS. A similar effect is described by Subrebost et al. (2002), where silicon is dry etched underneath a layer of PDMS. This problem is exacerbated by the fact that the PDMS etch rate, which starts at approximately 18 $\mu\text{m}/\text{h}$, decreases as the PDMS layer thins to about 1 μm . This allows ample time for the RIE to attack the gold film underlying the permeable PDMS layer.

Because of high selectivity of our recipe shown in Table 2b and c, the RIE can run approximately 1.5 times as long as typically necessary without danger of over-etching into the gold. This is important because the exact time needed to fully etch is difficult to determine: not only do loading effects change the etch rate, but, in the presented fabrication process, the PDMS layer is not always exactly the same thickness from one device to another.

Another advantage of the recipes shown in Table 2b and c is that they do not etch aluminum at an appreciable rate as does the recipe shown in Table 2a (Garra et al. 2002; Shao and Miller 2007), so the 1,500 Å mask holds up for over 6 h. Incidentally, we tested the same recipe with SF_6 in place of CF_4 and it also gave satisfactory results. Our primary goals were reliability and repeatability rather than speed, but we suspect that more future work could be done to optimize the speed of the RIE process and still maintain feature precision.

Testing indicates that our novel dry etch process works reliably. Figure 2 shows a Scanning Electrode Microscope

Table 2 Parameters used for reactive ion etching process

	Gas pressure (mTorr)	RF level (W)	O_2 flow rate	CF_4 flow rate	PDMS etch rate ($\mu\text{m}/\text{h}$)	Etches underlying gold:
(a) PDMS etch, rate-optimized	47	270	25% (50 sccm)	75% (12.5 sccm)	18	Quickly
(b) Our step 1	200	70	90% (27 sccm)	10% (3 sccm)	2 (approximate)	Slightly
(c) Our step 2	200	70	97% (29 sccm)	3% (1 sccm)	1 (approximate)	Negligibly

We use a customized, two-step process that etches holes in the upper PDMS layer of our device without damaging the underlying gold electrodes.

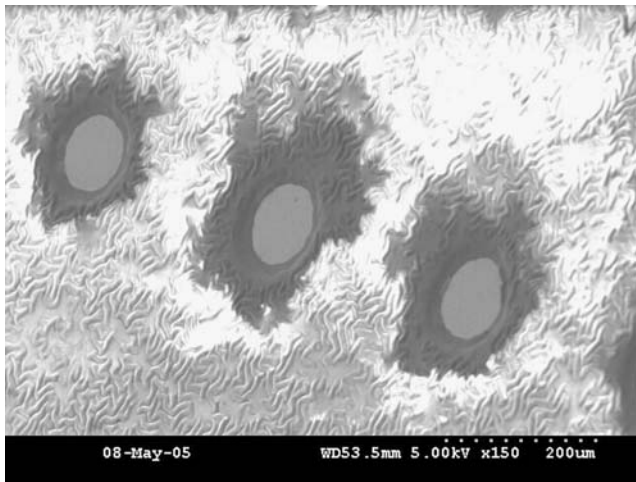


Fig. 2 Scanning electron microscope image of etched electrode contacts. Three PDMS-substrate MEA electrodes are shown following the reactive ion etch step. The upper PDMS layer has been etched to expose the underlying gold electrode contacts (*circular areas above*) without incurring any damage to the gold. The *lighter area* indicates the prior presence of an aluminum mask, which was used to prevent etching of the PDMS insulation over electrode wires and was subsequently stripped before imaging

image of orifices etched through PDMS with our recipe; it can be seen that the underlying gold film is cleanly exposed and intact.

2.7 Step 7. Stripping of aluminum layer

Following the dry etch of holes into the insulating PDMS layer, we strip the protective aluminum mask layer in a bath of aluminum etchant. During this process, we ramp the bath temperature from 25 to 70 °C (Fig. 1(h)).

2.8 Step 8. Removal from slide

To reduce the force required to remove the finished MEA from the glass slide, we first excise the 3 mm array border that is on bare glass. For subsequent manual removal of the array from the glass slide, we wedge a razor blade under a corner to start the delamination and then very gently peel off the device by hand (Fig. 1(i)). We then soak the MEA in deionized water for a minimum of 24 h to remove any residual fabrication chemicals before *in vitro* use. Figure 3 shows an initial functional prototype of the completed PDMS-based MEA.

3 Array evaluation

In order to assess the capabilities and limitations of our fabricated MEA, we conducted a series of electrical, mechanical, and neural interfacing tests. These tests were designed to assess the MEA under conditions pertinent to

its imminent use as an *in vitro* electrophysiology tool. Neural interfacing assessment focused on measuring the MEA's ability to selectively activate white matter tracts when wrapped around an *in vitro* isolated rat spinal cord, as this will be the first *in vitro* application for which the MEA will be used.

3.1 Electro-mechanical testing

We characterized the electrical impedances of exposed electrodes and insulation for each of five traces on four fabricated MEAs (19 traces total). We measured impedances using a spectrum analyzer (SRS Dynamic Signal Analyzer, SR785) at frequencies from 100 Hz to 100 kHz. For all experiments, electrical interfacing between spectrum analyzer and MEA was accomplished using silver wire leads, the first of which was pressed onto a given electrode trace's exposed contact pad. To connect electrically with either the exposed electrodes or insulated wire traces, the other lead was lowered into drops of Hanks' Balanced Salt

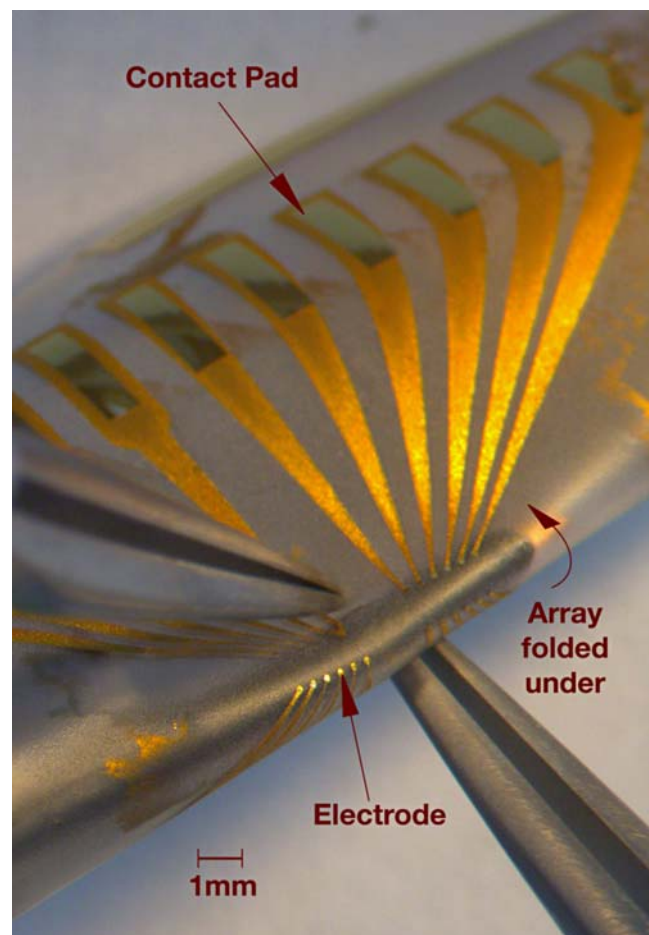


Fig. 3 Fabricated PDMS-substrate MEA. A final product of our fabrication process is shown wrapped around a wire of similar diameter (2 mm) to that of the neonatal intact or hemisectioned juvenile *in vitro* rat spinal cord

Solution (HBSS 1X, Gibco) [(in mM): KCl 5.33, KH_2PO_4 0.441, NaCl 137.93, NaHCO_3 4.17, Na_2HPO_4 , D-glucose 5.56, Phenol Red 0.0266] that had been placed over the relevant sites (Fig. 4). This method resulted in a much higher recorded impedance than that of the gold traces themselves, due to the gold/HBSS and HBSS/wire interfacial resistance; regardless, this was an effective method for evaluating conductivity without damaging electrode exposures through rough contact with spectrum analyzer leads. Results for impedance testing of the electrode contacts and insulated wire traces are given in Fig. 5, and show that the electrode impedances are uniform across electrodes and compare favorably to properties of rigid-MEA electrodes (Heuschkel et al. 2002; Oka et al. 1999). Impedance measurement results also indicate that the PDMS insulating layer acts well as an insulator (Fig. 5(a)).

As an additional proof-of-concept, elasticity of the MEA was evaluated by measuring the impedance properties of the device's electrodes both during and after repeated uniaxial loading. In addition to testing a straight-trace electrode design (one trace on one array), two types of serpentine electrode trace patterns were evaluated (parallel and intersecting, Fig. 7(a)). One trace each of the serpentine patterns was tested. To stretch the MEA, we used a custom-built apparatus that clamped to two ends of the array (Fig. 6). The stretching device was used to manually

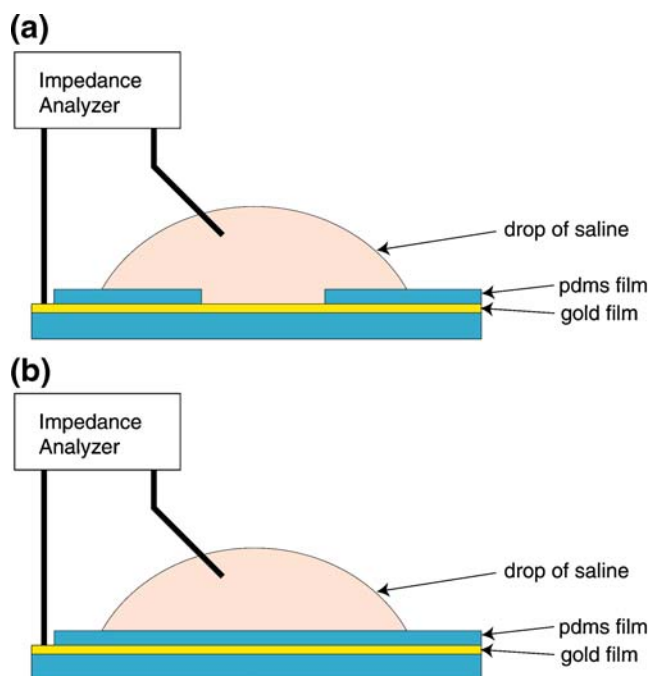


Fig. 4 Experimental apparatus for electrical evaluation of MEA. To evaluate the electrical properties of the MEA, we measured impedances using a spectrum analyzer at frequencies from 100 Hz to 100 kHz. A drop of Hanks' Balanced Salt Solution was used to interface between the MEA and the spectrum analyzer lead (0.015 in. silver wire). Configurations for measuring impedance of an electrode contact (a) and the insulating PDMS film (b) are shown

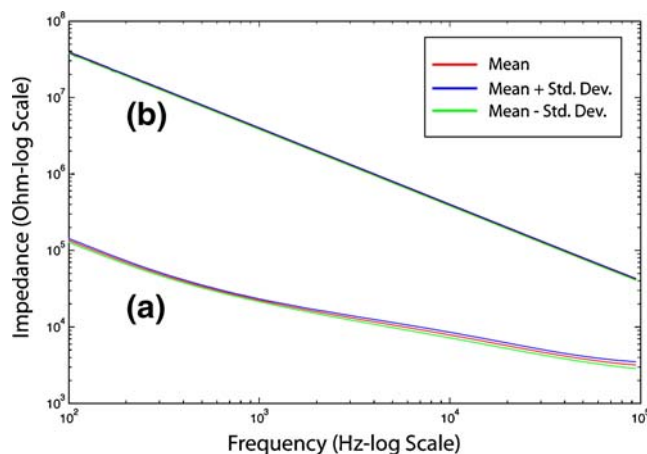


Fig. 5 Results for electrical impedance testing of 19 MEA electrodes on four arrays. The MEA electrodes consistently exhibited impedance values comparable to those of rigid MEAs (Heuschkel et al. 2002; Oka et al. 1999) (a) and the PDMS-covered traces demonstrated impedance values indicative of insulation (b)

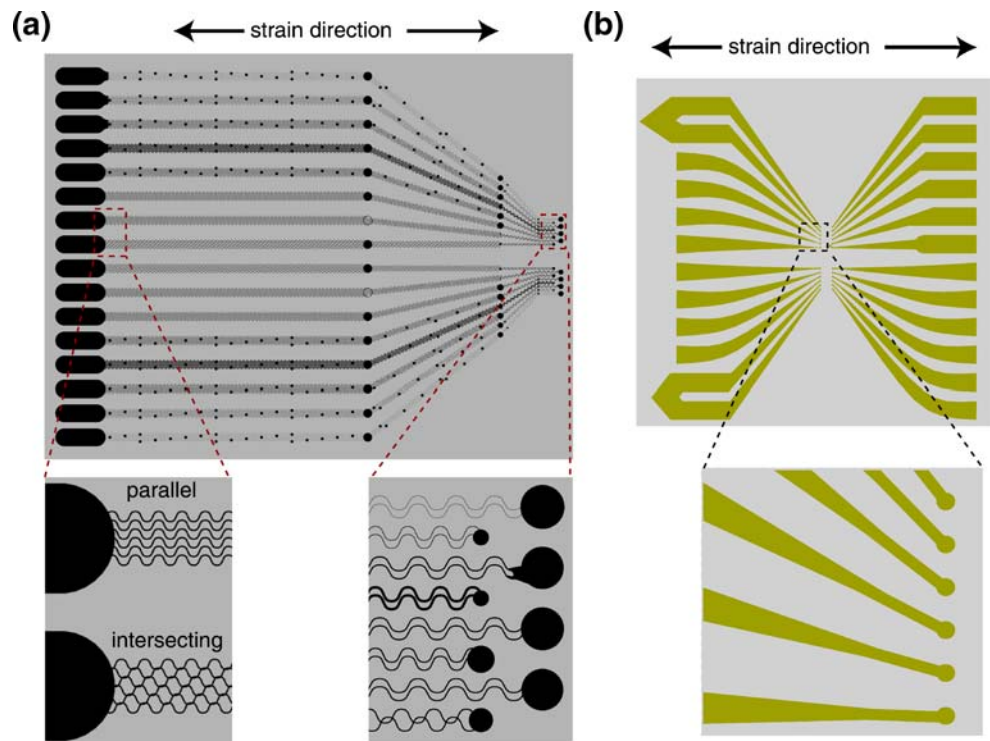
increase the strain along the length of the electrode traces at intervals of 1%. At each stretching increment, impedances were measured at frequencies ranging from 100 Hz to 100 kHz. Our measurements were not precise enough to detect the continuous increase in impedance accompanied by strain near the failure point, but were sufficient to measure total trace failure. Impedance of 60 k Ω or less was considered acceptable; when failure occurred, the impedance rose by a factor of approximately 100.

We found that the intersecting serpentine electrode trace design shown in Fig. 7 performed better than the other tested patterns, withstanding 8% strain while continuing to conduct at impedances similar to rigid MEA electrodes. Serpentine traces performed better than straight electrode traces (Fig. 7), which failed at 3% strain. These observed strain limits are lower than those reported for other, PDMS-



Fig. 6 Uniaxial strain device for electro-mechanical evaluation of the PDMS-based MEA. The custom-made apparatus shown was used to clamp the MEAs and apply uniaxial strain in 1% increments

Fig. 7 Serpentine Trace Design for MEA Electrode Traces. **(a)** An intersecting, serpentine electrode trace pattern confers a greater elasticity to the PDMS-based MEA (electrode trace conductivity failure at >8% strain for one tested trace, recoverable upon relaxation) than does a **(b)** non-serpentine pattern of electrode traces (failure at >3% strain, no recovery, one tested trace). The parallel, serpentine electrode trace pattern shown in **(a)** conferred no functional elasticity advantages when compared to the non-serpentine pattern **(b)**



based stretchable electrodes that have been designed for the study of traumatic brain injury (Tsay et al. 2007; Yu et al. 2007). Nonetheless, these strain limits appear to be above those imposed upon the devices during repetitive use as a conformable, multi-electrode interface to the *in vitro* spinal cord, as over repetitive interfacing use, the MEAs have not failed due to excessive strain.

We also tested the ability of the PDMS substrate to conform to shapes similar to that of our targeted neural substrate (the *in vitro* isolated spinal cord). Arrays fabricated using both PDMS and polyimide as substrates were wrapped around plastic tubing of diameter (2 mm) similar to that of the isolated neonatal rat spinal cord and the hemisected juvenile rat spinal cord. Figure 8(a) demonstrates the superior conformability of a PDMS film to the bending tube, while Fig. 8(b) shows a polyimide film bending and folding in multiple places, providing a less continuous contact with the bending tube surface.

3.2 Neural interfacing

One experiment was performed to demonstrate the capacity of our elastic MEA to activate a specific region of longitudinally-oriented axonal bundles (spinal white matter tracts) in the *in vitro* rat isolated spinal cord (Fig. 9). We determined this degree of selectivity by delivering single-site MEA stimuli to the surface of the cord and then recording the evoked compound action potential (CAP) response 11.5 mm distal to the site of activation (on adjacent white matter tracts). To determine stimulus

selectivity, we measured the strength of evoked CAPs as we increased recorded lateral distance from the site of maximal white matter tract CAP activation.

To prepare for *in vitro* spinal cord interfacing, we used a protocol adapted from Shay et al. (Shay et al. 2005), in which a juvenile (postnatal day 11) Sprague–Dawley rat was first anesthetized with 10% wt./vol. urethane (2.0 mg/kg injected intraperitoneally) and then submerged in an ice

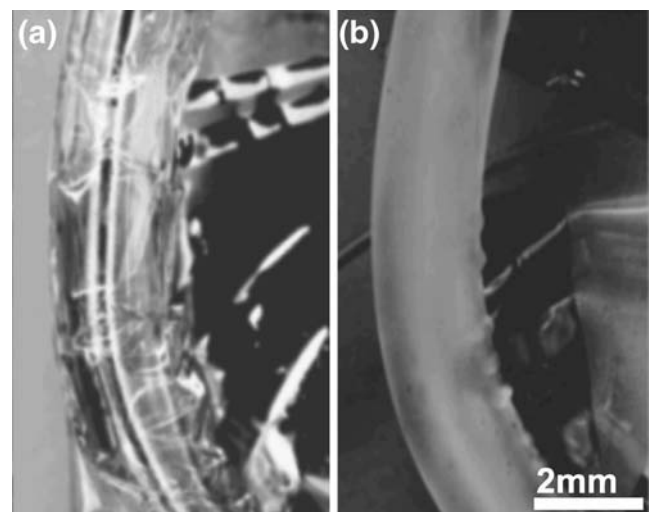


Fig. 8 Bending of polyimide and PDMS arrays. We visually compared the ability of PDMS and polyimide array substrates to conform to a bending tube of the same approximate diameter as our *in vitro* spinal cords. **(a)** Polyimide film wrapped around a 2 mm-diameter tube shows buckling of the polyimide film along the tube. **(b)** PDMS film wrapped around a 2 mm tube conforms more uniformly to the bending tube

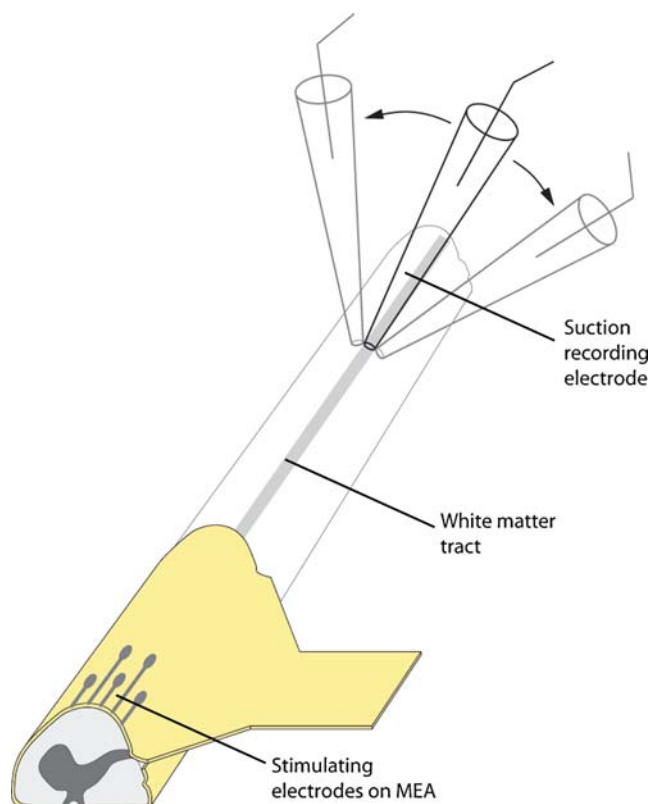


Fig. 9 Experimental setup for surface stimulation of the *in vitro* isolated rat spinal cord (hemisected). The MEA was wrapped around the isolated *in vitro* spinal cord of a postnatal day 11 rat and two adjacent MEA electrodes (bipolar configuration) were used to stimulate the fifth thoracic segment's ventrolateral funiculus. The degree of stimulus spread was assessed by recording surface compound action potentials (CAPs) at multiple circumferential sites distant to the site of activation. For recording, a glass suction electrode (40–50 μm internal diameter) was placed 11.5 mm caudal to the stimulation site to record CAP responses in 50 μm lateral increments from the site of the peak response

slurry for 5 min to decrease body temperature. Following decapitation, the cervical to sacral spinal cord was isolated along with ventral and dorsal roots. The cord was then pinned ventral-side up in a Sylgard-coated (Dow Corning) Petri dish containing cold (4 $^{\circ}\text{C}$), oxygenated (95% O_2 , 5% CO_2) high sucrose-containing solution [(in mM): sucrose 250; KCl 2.5; NaHCO_3 26; NaH_2PO_4 1.25; D-glucose 25; MgCl_2 3; CaCl_2 1]. Spinal cord dura was carefully removed and a sagittal hemisection was performed using insect pins (1.0 mm, Fine Science Tools). The spinal cord was then placed in room-temperature, oxygenated (95% O_2 , 5% CO_2), artificial cerebrospinal fluid (aCSF, in mM: NaCl 128; KCl 1.9; D-glucose 10; MgSO_4 1.3; CaCl_2 2.4; KH_2PO_4 1.2; and NaHCO_3 26) and allowed to equilibrate for 1 h prior to further experimentation.

To prepare for stimulation and recording, the MEA was connected to an STG-2008 stimulation unit (MultiChannel Systems) using a custom-built press fit connector. Exposed electrodes on the MEA were then wrapped around the fifth

thoracic segment of the cord such that the stimulating electrodes were on the ventrolateral funiculus (Fig. 9). To secure the MEA in this configuration, insect pins (1.0 mm, Fine Science Tools) were used to pin non-electrode containing parts of the MEA (i.e. flaps of PDMS film adjacent to the MEA electrode traces) to the bottom of the dish. A reference ground electrode was placed in the bath near the caudal end of the spinal cord. A glass suction electrode (40–50 μm internal diameter) was used to record stimulus-evoked CAPs as they conducted along the surface of the spinal cord white matter. This electrode made bipolar recordings using chloridated silver wires: one placed within the glass and the other placed immediately outside the glass.

Two adjacent MEA electrodes were used to deliver a single, bipolar, charge-balanced current pulse to the surface of the spinal cord. To measure the subsequent evoked CAP, a recording electrode was placed 11.5 mm caudal to the stimulation site, starting at the circumferential location that responded with the greatest evoked CAP response. The minimum current value at which a CAP was visible at this recording site was defined as the threshold stimulus value (for this experiment, 700 $\mu\text{A}/500 \mu\text{s}$). Between single-pulse stimuli at this threshold value (and several values greater than threshold, increasing in 20 μA increments), the recording electrode was moved in 50 μm lateral increments from the site of the peak response to record CAP responses on laterally adjacent tracts. The strength of the evoked CAP response at these different sites along the cord was calculated based on the baseline-subtracted, rectified and integrated signal ($\mu\text{V} \cdot \mu\text{s}$) averaged over ten trials for each recording site (Fig. 10, standard error bars shown).

Results indicate that, for reliable activation of visible CAP responses along the ventrolateral funiculus, the minimum charge-balanced current pulse required using our MEA was 700 $\mu\text{A}/500 \mu\text{s}$. This compares to a threshold value of 300 $\mu\text{A}/100 \mu\text{s}$ determined using a conventional bipolar tungsten electrode (5 μm tip diameter, 10 μm inter-electrode distance) pressed firmly onto the cord surface. When the MEA was not placed conformably around the cord but instead placed loosely on top of the cord within the aCSF bath, no recruitment of white matter tracts was discernable at any single-pulse, bipolar-configuration current value within the range of our stimulator (800 $\mu\text{A}/200 \text{ms}$).

Selectivity of tract stimulation using the MEA was demonstrated with a decremented—and eventually absent—evoked CAP on laterally adjacent axonal tracts (Fig. 10). The stimulus selectivity of the MEA compared favorably to that evoked with a tungsten bipolar stimulating electrode (Fig. 10), in that the rate at which evoked CAP response strength decreased over recording distance compared favorably to the trendline for threshold stimulation with a bipolar tungsten electrode control ($R^2=0.8201$). These results indicate a similarity in the stimulus selectivity

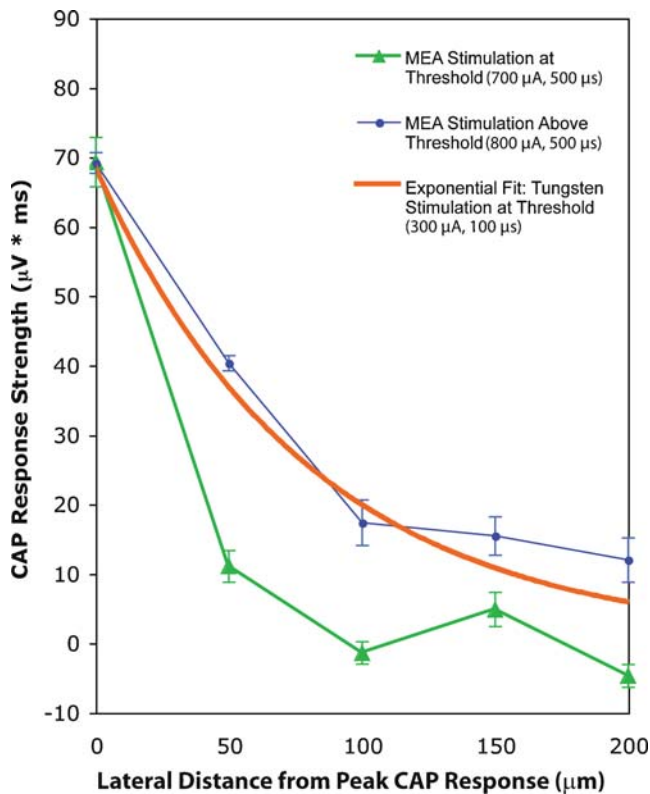


Fig. 10 Spinal cord white matter response to MEA surface stimulation

between the MEA and a conventional bipolar tungsten electrode in direct contact with the spinal cord surface. At stimulus values incrementally greater than threshold value for the MEA, we observed incrementally greater recruitment of white matter tracts (as shown by higher-strength CAP responses, Fig. 10).

MEA (vs. tungsten control) stimulus-evoked compound action potentials (CAPs) on white matter tracts are plotted over lateral recording distance from the site of peak CAP response, for one array wrapped around the thoracic region of one *in vitro* spinal cord. Recordings were made 11.5 mm caudal to the site of ventrolateral funiculus stimulation, in 50 µm lateral increments. Strength of CAP response was quantified by finding the area under the baseline-subtracted, rectified traces of the CAP recording. Shown are responses to MEA stimuli at threshold value (700 µA/500 µs single current pulse) as well as at 800 µA/500 µs, demonstrating an increase in white matter tract recruitment at greater stimulus values. To compare stimulus selectivity, also shown is the logarithmic trendline for threshold stimulation (300 µA/100 µs) using a conventional tungsten bipolar electrode. The rate at which evoked CAP response strength decreased over recording distance compared well to the logarithmic trendline for tungsten bipolar stimulation ($R^2=0.8201$), indicating a similar stimulus selectivity between the two methods.

4 Discussion

An ongoing challenge among neural interfacing techniques is maximizing selectivity of activation while minimizing invasiveness and damage to the interfaced tissue. In this paper, we propose surface stimulation of axonal tracts as an approach to achieving this balance for the activation of discrete pathways with actions on spinal cord functional systems. We present, for this application, a technique for stimulating surface tracts with an MEA that uses a conformable-substrate in order to promote precise stimulus delivery to the cord surface. We use PDMS as a substrate because of its superior elasticity and, to achieve a small electrode feature size, describe a new, scalable, fabrication process for creating a high electrode density, elastic MEA on PDMS substrate.

Our fabrication approach enables reliable and rapid production of MEAs with various desired electrode geometries and includes a novel reactive ion etch (RIE) process that makes possible our 60 µm diameter electrode resolution. To date, we have fabricated approximately 40 arrays (three different designs) with a success rate of roughly 80%. Our fabrication process differs from previous work in silicone micro-array fabrication in that we use a customized reactive ion etch process for opening electrode and electrical contact orifices in a membrane of PDMS. This process removes PDMS cleanly and does not etch away the underlying gold electrode. To our knowledge, no previously published RIE recipes for dry etching PDMS are capable of selectively removing the PDMS and leaving an underlying gold thin film intact.

Also novel to PDMS MEAs, we use serpentine electrode traces to increase overall elasticity of the electrode array. Although PDMS stretches easily, metal traces have limited the elasticity of previous silicone MEAs (Maghribi et al. 2002; Schuettler et al. 2005). Gold serpentine traces on silicone have been investigated (Gray et al. 2004; Madou 2002), but they have not previously been incorporated into a stretchable multi-channel electrode array. We have shown with initial studies that traces with intersecting serpentine patterns were capable of stretching 8% without failure, compared with a 3% stretching limit for MEAs with straight electrode traces of the same composition. These preliminary results show an advantage of intersecting serpentine trace geometries over those of straight traces for the purposes of MEA stretchability. Future studies are planned to more fully characterize and optimize the elasticity of our PDMS MEA, whose design is not as stretchable as other PDMS MEAs, such as those used for studying traumatic brain injury (withstanding up to 20% uniaxial strain (Tsay et al. 2007; Yu et al. 2007)). For our *in vitro* spinal cord interfacing work thus far, however, the elasticity of both the intersecting serpentine-trace and straight-trace MEAs has been sufficient for repetitive handling and use, and the smaller electrode

feature size has been advantageous for our stimulus locations and protocol.

We demonstrated that our fabrication process produces MEAs with uniform electrical properties and that our devices can selectively activate white matter tracts in the *in vitro* isolated spinal cord. Initial results indicate that a close, conformable fit of the array to the surface of the cord is critical to the MEA's ability to evoke compound action potentials with spatial precision, presumably because it gives the stimulating electrodes a closer, semi-isolated proximity to the cord surface. We are in the process of conducting a more extensive evaluation of the role of the MEA substrate in promoting selective activation of white matter tracts, especially in relation to flexible-substrate (but non-elastic) MEAs. Furthermore, we plan to assess the electrical and mechanical stability of the MEA over extended usage and incubation periods as a first step towards determining its potential as an *in vivo* device.

Future MEA design improvements will focus on augmenting the isolated delivery of electrical stimuli to the cord surface, using techniques including fabrication of raised PDMS isolation wells around individual electrodes. We will also be applying modified geometries of single electrodes and multiple electrode configurations and evaluating their influence on MEA stimulus selectivity. Our ultimate goal is to use this technology as part of a multi-site interface for selective, closed-loop recruitment and control of spinal cord functional systems.

Acknowledgements We thank James Ross for discussions regarding fabrication strategies, Bao To for machining and assembling initial versions of the clamping connector., J.Mark Meacham for illustration software help, and Jevin Scrivens, Edgar Brown, and Shane Migliore for advice about building and using the strain tester. This work was supported by NIH Grant EB00786-01, NSF IBN-0349042, and NIH Grant EB006179.

References

- D. Armani, C. Liu, N. Aluru. in *Micro Electro Mechanical Systems, 1999. MEMS '99*. Twelfth IEEE International Conference on. 1999, p. 222
- A. Branner, R.B. Stein, R.A. Normann, J. Neurophysiol. **85**, 1585 (2001)
- G.S. Brindley, C.E. Polkey, D.N. Rushton, Paraplegia **20**, 365 (1982)
- H.L. Cater, D. Gitterman, S.M. Davis, C.D. Benham, B. Morrison 3rd, L.E. Sundstrom, J. Neurochem. **101**, 434 (2007)
- J.K. Chapin, Curr. Opin. Neurol. **13**, 671 (2000)
- G.M. Clark, Y.C. Tong, R. Black, I.C. Forster, J.F. Patrick, D.J. Dewhurst, J. Laryngol. Otol. **91**, 935 (1977)
- A.F. DiMarco, J. Rehabil. Res. Dev. **38**, 601 (2001)
- D.J. Edell, V.V. Toi, V.M. McNeil, L.D. Clark, IEEE Trans. Biomed. Eng. **39**, 635 (1992)
- J. Garra, T. Long, J. Currie, T. Schneider, R. White, M. Paranjape, J. Vac. Sci. Technol. A Vac. Surf. Films **20**, 975 (2002)
- Y.P. Gerasimenko, I.A. Lavrov, G. Courtine, R.M. Ichiyama, C.J. Dy, H. Zhong, R.R. Roy, V.R. Edgerton, J. Neurosci. Methods **157**, 253 (2006)
- D.S. Gray, J. Tien, C.S. Chen, Adv. Mater. **16**, 393 (2004).
- W.M. Grill, M.D. Craggs, R.D. Foreman, C.L. Ludlow, J.L. Buller, J. Rehabil. Res. Dev. **38**, 641 (2001)
- W. He, R.V. Bellamkonda, Biomaterials **26**, 2983 (2005)
- M.O. Heuschkel, M. Fejtl, M. Raggenbass, D. Bertrand, P. Renaud, J. Neurosci. Methods **114**, 135 (2002)
- T. Hillman, A.N. Badi, R.A. Normann, T. Kertesz, C. Shelton, Otol. Neurotol. **24**, 764 (2003)
- Y.H. Holman G., R.C.W., A.O.D. Willows, D. Denton, K.F. Bohringer, in IEEE-EMBS Second Annual International Special Topic Conference on Microtechnologies in Medicine & Biology, Madison, WI, USA (2002)
- R.M. Ichiyama, Y.P. Gerasimenko, H. Zhong, R.R. Roy, V.R. Edgerton, Neurosci. Lett. **383**, 339 (2005)
- D.K. Kessler, Ann. Otol. Rhinol. Laryngol. Suppl. **177**, 8 (1999)
- G.H. Kraft, S.S. Fitts, M.C. Hammond, Arch. Phys. Med. Rehabil. **73**, 220 (1992)
- A. Kralj, T. Bajd, R. Turk, Clin. Orthop. Relat. Res. **233**, 34 (1988)
- D.K. Leventhal, D.M. Durand, Ann. Biomed. Eng. **31**, 643 (2003)
- D.K. Leventhal, D.M. Durand, IEEE Trans. Biomed. Eng. **51**, 1649 (2004)
- W.T. Liberson, H.J. Holmquest, D. Scot, M. Dow, Arch. Phys. Med. Rehabil. **42**, 101 (1961)
- G.E. Loeb, R.A. Peck, J. Neurosci. Methods **64**, 95 (1996)
- M.J. Madou, *Fundamentals of Microfabrication: The Science of Miniaturization*, 2nd edn. (CRC, 2002)
- M. Maghribi, J. Hamilton, D. Polla, K. Rose, T. Wilson, P. Krulevitch, in *Microtechnologies in Medicine & Biology 2nd Annual International IEEE-EMB Special Topic Conference on, Madison, WI*, ed. by A. Dittmar, D. Beebe (IEEE, Piscataway, 2002), p. 80
- D.S. Magnuson, T.C. Trinder, J. Neurophysiol. **77**, 200 (1997)
- D.S. Magnuson, M.J. Schramm, J.N. MacLean, Neurosci. Lett. **192**, 97 (1995)
- D. McDonnall, G.A. Clark, R.A. Normann, IEEE Trans. Neural Syst. Rehabil. Eng. **12**, 208 (2004)
- G.G. Naples, J.T. Mortimer, A. Scheiner, J.D. Sweeney, IEEE Trans. Biomed. Eng. **35**, 905 (1988)
- H. Oka, K. Shimono, R. Ogawa, H. Sugihara, M. Taketani, J. Neurosci. Methods **93**, 61 (1999)
- V.S. Polikov, P.A. Tresco, W.M. Reichert, J. Neurosci. Methods **148**, 1 (2005).
- A. Prochazka, M. Gauthier, M. Wieler, Z. Kenwell, Arch. Phys. Med. Rehabil. **78**, 608 (1997)
- A. Prochazka, V.K. Mushahwar, D.B. McCreery, J. Physiol. **533**, 99 (2001)
- D.C. Rodger, W. Li, A.J. Fong, H. Ameri, E. Meng, J.W. Burdick, R.R. Roy, V.R. Edgerton, J.D. Weiland, M.S. Humayun, Y. Tai, in *IEEE Engineering in Medicine and Biology Society Special Topic Conference on Microtechnologies in Medicine and Biology*, Okinawa, Japan 2006
- P.J. Rousche, D.S. Pellinen, D.P. Pivin Jr., J.C. Williams, R.J. Vetter, D.R. Kipke, IEEE Trans. Biomed. Eng. **48**, 361 (2001)
- M. Sahin, M.A. Haxhiu, D.M. Durand, I.A. Dreshaj, J. Appl. Physiol. **83**, 317 (1997)
- S. Schmidt, K. Horch, R. Normann, J. Biomed. Mater. Res. **27**, 1393 (1993).
- M. Schuettler, T. Stieglitz, *5th Annual International Conference of the International Functional Electrical Stimulation Society*, Aalborg, Denmark, 18 2000
- M. Schuettler, S. Stieess, B.V. King, G.J. Suaning, J. Neural Eng. **2**, S121 (2005)

- J. Shao, E. Miller. Releasing Polydimethylsiloxane (PDMS) Replica Parts From Micromolds, 2007, from <http://www.pnl.gov/microproducts/conferences/2004/posters/shao.pdf>
- B.L. Shay, M. Sawchuk, D.W. Machacek, S. Hochman, J. Neurophysiol. **94**, 2867 (2005)
- F.A. Spelman, IEEE Eng. Med. Biol. Mag. **18**, 27 (1999)
- R.B. Stein, V. Mushahwar, Trends Neurosci. **28**, 518 (2005)
- R.B. Stein, K.G. Pearson, J. Theor. Biol. **32**, 539 (1971)
- T. Stieglitz (2001). Catalogue on Available Flexible, Light-weighted Microelectrodes, from www.ibmt.fraunhofer.de/gruppe_1/download/IBMT_Neuro%20Electrode%20Catalogue%20-%20July%202001.pdf
- J.J. Struijk, M. Thomsen, J.O. Larsen, T. Sinkjaer, IEEE Eng. Med. Biol. Mag. **18**, 91 (1999)
- G.L. Subrebost, A.J. Rosenbloom, V. Weedn, K. Gabriel, in *Proceedings of the Sixth International Symposium on Micro Total Analysis System (mTAS 2002)*, Nara, Japan, Nov. 2–8, 2002
- Y.Y.-C.T. Suzuki, in *Micro Electro Mechanical Systems, IEEE The Sixteenth Annual International Conference on*, Kyoto 2003
- P.N. Taylor, J.H. Burrige, A.L. Dunkerley, A. Lamb, D.E. Wood, J.A. Norton, I.D. Swain, Clin. Rehabil. **13**, 439 (1999)
- C. Tsay, S.P. Lacour, S. Wagner, B. Morrison III, in *Sensors, 2005 IEEE2005*, p. 1169
- C. Tsay, O. Graudejus, S. Wagner, S.P. Lacour, B. Morrison III, in *MRS Proceedings, Symposium U: Advanced Materials for Neuroprosthetic Interfaces*, San Francisco, CA 2007
- D.J. Tyler, D.M. Durand, IEEE Trans. Neural Syst. Rehabil. Eng. **10**, 294 (2002)
- H.P. Weingarden, G. Zeilig, R. Heruti, Y. Shemesh, A. Ohry, A. Dar, D. Katz, R. Nathan, A. Smith, Am. J. Phys. Med. Rehabil. **77**, 276 (1998)
- X. Yang, C. Grosjean, Y.C. Tai, in *Solid-state Sensor and Actuator Workshop*, 1998
- Z. Yu, O. Graudejus, C. Tsay, S.P. Lacour, S. Wagner, B. Morrison III, in *MRS Proceedings, Symposium U: Advanced Materials for Neuroprosthetic Interfaces*, 2007
- Y. Zhong, X. Yu, R. Gilbert, R.V. Bellamkonda, J. Rehabil. Res. Dev. **38**, 627 (2001)